# APPLICATION OF THE VORTEX-LATTICE TECHNIQUE TO THE ANALYSIS OF THIN WINGS WITH VORTEX SEPARATION AND THICK MULTI-ELEMENT WINGS

Charles W. Smith and Ishwar C. Bhateley
Fort Worth Division of General Dynamics

## SUMMARY

Two techniques for extending the range of applicability of the basic vortex-lattice method are discussed. The first technique improves the computation of aerodynamic forces on thin, low-aspect-ratio wings of arbitrary planforms at subsonic Mach numbers by including the effects of leading-edge and tip vortex separation, characteristic of this type wing, through use of the well-known suction-analogy method of E. C. Polhamus. Comparisons with experimental data for a variety of planforms are presented.

The second technique consists of the use of the vortex-lattice method to predict pressure distributions over thick multi-element wings (wings with leading- and trailing-edge devices). A method of laying out the lattice is described which gives accurate pressures on the top and part of the bottom surface of the wing. Limited comparisons between the result predicted by this method, the conventional lattice arrangement method, experimental data, and 2-D potential flow analysis techniques are presented.



## INTRODUCTION

Vortex-lattice methods are known to give reasonable results for thin wings of moderate to high aspect ratio. However, use of these methods to predict the aerodynamic forces on low-aspect-ratio wings has not been practical due to the significant vortex lift generated by these wings. The analysis and prediction of the nonlinearities associated with the vortex lift has received considerable attention in the literature for many years. Methods of solution based on complex mathematical models have generally failed. However, within the past several years, E. C. Polhamus of the NASA Langley Research Center has proposed and verified through comparison with experimental data an analytical method for sharp-leading-edge wings of zero taper ratio (reference 1). The

method is based on a leading-edge suction analogy proposed by Polhamus in reference 2. Extension of the suction analogy to plane rectangular rings has been accomplished by J. E. Lamar in reference 3. A method for calculating the lift, drag, and pitching moment of cambered, sharp-edged wings of arbitrary planform is presented here as a logical extension of the suction-analogy concept. A vortex-lattice program is utilized to provide the potential-flow force coefficients required by the suction-analogy concept and to provide the foundation for development of a computer procedure which incorporates the methods developed.

The accurate calculation of pressure distributions near the leading edge of thick multi-element wings is of considerable interest to the aerodynamicist. Vortex-lattice methods using the conventional vortex-lattice arrangement of distributing the vorticity on the camber surface yield pressure coefficients which approach infinity at the leading edge due to the singularity at the leading edge. An alternate method of laying out the lattice is described which circumvents this difficulty and gives reasonable predictions for the pressures on the top surface and a part of the bottom surface of wings.

## SYMBOLS

Values are given in both SI and U.S. Customary Units. The measurements and calculations were made in U.S. Customary Units.

| | |
|---|---|
| AR | aspect ratio |
| $\bar{c}$ | mean aerodynamic chord, cm (in.) |
| $C_A$ | axial-force coefficient |
| $C_{D_L}$ | drag-due-to-lift coefficient |
| $C_L$ | total lift coefficient ($C_{L_p} + C_{L_v}$) |
| $C_{L_p}$ | zero-suction potential-flow lift coefficient |
| $C_{L_v}$ | vortex-lift coefficient |
| $C_m$ | total pitching-moment coefficient |
| $C_{m_p}$ | zero-suction potential-flow pitching-moment coefficient for half-span wing |

| | |
|---|---|
| $C_N$ | normal-force coefficient |
| $C_{N_p}$ | potential-flow normal-force coefficient for half-span wing |
| $C_P$ | pressure coefficient |
| $C_S$ | potential-flow leading-edge suction coefficient for half-span wing |
| $C_T$ | potential-flow leading-edge thrust coefficient for half-span wing |
| $C_Y$ | potential-flow side-force coefficient for half-span wing |
| $C_{Y_2}$ | potential-flow side-force-coefficient contribution from streamwise members of the vortex lattice for half-span wing |
| $C_\mu$ | nozzle momentum coefficient |
| $K_p$ | potential-flow normal-force slope |
| $(K_p)_m$ | potential-flow constant used in pitching-moment calculation |
| $K_v$ | vortex-lift constant |
| $K_{v_{LE}}$ | leading-edge vortex-lift constant used in lift calculation |
| $(K_{v_{LE}})_m$ | leading-edge vortex-lift constant used in pitching-moment calculations |
| $K_{v_{TIP}}$ | tip vortex-lift constant used in lift calculations |
| $(K_{v_{TIP}})_m$ | tip vortex-lift constant used in pitching-moment calculations |
| M | Mach number |
| $x_m$ | pitching-moment arm for tip vortex-lift contributions, cm (in.) |
| $x_n$ | pitching-moment arm for leading-edge vortex-lift contributions, cm (in.) |

| | |
|---|---|
| $x/c$ | nondimensionalized chordwise location |
| $z_n$ | pitching-moment arm for leading-edge suction force, cm (in.) |
| $\alpha$ | angle of attack, degrees |
| $\lambda$ | planform taper ratio |
| $\Lambda$ | leading-edge sweep angle, degrees |
| $\phi$ | slope of the mean line perpendicular to the planform leading edge, degrees |

## THEORETICAL DEVELOPMENT FOR THIN WINGS

### The Polhamus Suction Analogy

The General Dynamics vortex-lattice method has been modified to incorporate the calculation of vortex separation effects.

The basis for this modification to the vortex-lattice procedure is the Polhamus leading-edge suction analogy, which is detailed in reference 2. Briefly, it is based on the postulate that the normal force on the upper surface is the same for attached vortex flow as the leading-edge suction force for attached potential flow. The total lift of sharp-edged, pointed-tip wings is given as

$$C_L = C_{L_p} + C_S \cos \alpha \tag{1}$$

where $C_{L_p}$ is the potential-flow lift and $C_S$ is the leading-edge suction force. Polhamus writes the lift in terms of K-factors, $K_p$ and $K_v$, which are functions of planform and Mach number only. That is,

$$C_L = K_p \sin \alpha \cos^2 \alpha + K_{v_{LE}} \sin^2 \alpha \cos \alpha \tag{2}$$

where $K_p$ is, by definition, the normal-force slope given by potential-flow theory,

$$K_p \equiv \frac{\partial C_{N_p}}{\partial \sin \alpha \cos \alpha} \tag{3}$$

and $K_{v_{LE}}$ is, by definition,

$$K_{v_{LE}} \equiv \frac{\partial C_S}{\partial \sin^2 \alpha} \tag{4}$$

J. E. Lamar extended the Polhamus concept to rectangular wings of low aspect ratio in work reported in reference 3. The equation is

$$C_L = C_{L_p} + C_S \cos \alpha + C_Y \cos \alpha \tag{5}$$

where $C_Y$ is twice the potential-flow side force for the half-wing. In terms of K-factors,

$$C_L = K_p \sin \alpha \cos^2 \alpha + (K_{v_{LE}} + K_{v_{TIP}}) \sin^2 \alpha \cos \alpha$$

where, by definition,

$$K_{v_{TIP}} \equiv \frac{\partial C_Y}{\partial \sin^2 \alpha} \tag{6}$$

and $K_p$ and $K_{v_{LE}}$ are given in equations (3) and (4).

## Extension to Arbitrary Flat-Plate Wings

The above equations have been extended (reference 4) to more complex planforms. For a trapezoidal planform, the finite tip effects are taken into account for defining the vortex-lift contribution as

$$C_{L_v} = \left[ \frac{C_T}{\cos \Lambda} + C_Y - C_T \tan \Lambda \right] \cos \alpha \tag{7}$$

The above formulation recognizes that part of the total wing side force acts on the swept leading edge as part of the leading-edge suction vector ($C_T/\cos \Lambda$), and that the remainder ($C_Y - C_T \tan \Lambda$) acts on the wing tip, as shown in figure 1(a).

Generalization of the above result to wings of arbitrary planform results in the following equation for the lift:

$$C_L = C_{L_p} + \left[ \sum_{n=1}^{N} \frac{C_{T_n}}{\cos \Lambda_n} + C_Y - \sum_{n=1}^{N} C_{T_n} \tan \Lambda_n \right] \cos \alpha \quad (8)$$

The notation is illustrated in figure 1(b). In terms of K-factors, the total lift is given by

$$C_L = K_p \sin \alpha \cos^2 \alpha + (K_{v_{LE}} + K_{v_{TIP}}) \sin^2 \alpha \cos \alpha \quad (9)$$

where

$$K_{v_{LE}} = \frac{\partial}{\partial \sin^2 \alpha} \left[ \sum_{n=1}^{N} \frac{C_{T_n}}{\cos \Lambda_n} \right] \quad (10)$$

and

$$K_{v_{TIP}} = \frac{\partial}{\partial \sin^2 \alpha} \left[ C_Y - \sum_{n=1}^{N} C_{T_n} \tan \Lambda_n \right] \quad (11)$$

The potential-flow in-plane force coefficients, $C_T$ and $C_Y$, are those computed by any accurate lifting-surface theory. In this application, they are obtained from a vortex-lattice procedure. Compressibility effects are included through use of the Goethert transformation.

The zero-leading-edge-suction drag due to lift for sharp-edged, uncambered wings is defined by

$$C_{D_L} = C_L \tan \alpha \quad (12)$$

where $C_L$ is the total lift coefficient as given by equation (9).

Extension of the above formulations for the calculation of lift to the calculation of pitching moment logically follows. As in the lift case, the pitching moment is comprised of potential-

flow and vortex contributions. In general form, the resulting equation is

$$C_m = C_{m_p} + \frac{1}{c}\left[\sum_{n=1}^{N} (C_{T_n}/\cos \Lambda_n)(x_n) + \sum_{m=1}^{M}\left( \sum_{1}^{N+1} C_{Y_2} \right)_m (x_m)\right] \quad (13)$$

The notation is illustrated in figure 1(b). The potential-flow moment, $C_{m_p}$, is the moment resulting from the potential-flow normal forces on each member of the lattice.

The moment resulting from the vortex lift is comprised of a leading-edge and a tip component. To determine the leading-edge contribution, the leading-edge vortex lift, as determined by the suction analogy ($C_{T_n}/\cos \Lambda_n$), is assumed to act precisely at the leading edge of each chordwise strip. The moment is then the sum of the products of these forces and the moment arms ($x_n$), defined as the distance from the midpoint of the leading edge of each chordwise strip to the reference location. The leading-edge force includes a portion of the side force ($C_{T_n} \tan \Lambda_n$). The remainder of the side force, which is equal to the contribution of the streamwise members of the vortex lattice, is noted as

$$\left( \sum_{1}^{N+1} C_{Y_2} \right)_m$$

for each spanwise strip. The sum of this remainder constitutes the total tip vortex lift. Thus the tip-vortex-lift contribution to the moment is the sum of the products of these forces and the moment arms ($x_m$), defined as the distance from the midpoint of the tip of each spanwise strip to the reference location.

In terms of K-factors,

$$(K_p)_m \equiv \frac{\partial C_{m_p}}{\partial \sin \alpha \cos \alpha} \quad (14)$$

$$(K_{v_{LE}})_m = \frac{\partial}{\partial \sin^2 \alpha} \left[ \sum_{n=1}^{N} \frac{C_{T_n}}{\cos \Lambda_n} (x_n/\bar{c}) \right] \quad (15)$$

and

$$(K_{v_{TIP}})_m = \frac{\partial}{\partial \sin^2 \alpha} \left[ \sum_{m=1}^{M} \left( \sum_{1}^{N+1} C_{Y_2} \right)_m (x_m/\bar{c}) \right] \quad (16)$$

The total moment is given by

$$C_m = (K_p)_m \sin \alpha \cos \alpha + \left[ (K_{v_{LE}})_m + (K_{v_{TIP}})_m \right] \sin^2 \alpha \quad (17)$$

## Extension to Cambered Wings

The basis for determining the force and moment coefficients for thin, cambered planforms is the hypothesis that the total suction force acts perpendicular to the slope of the mean line at the leading edge. This is a logical extension to the suction-analogy assumption that the suction force acts in the normal-force direction for flat-plate planforms. Thus for cambered planforms, contributions to both the normal force and the axial force (in the suction direction) are realized from the total suction force calculated by potential-flow theory.

The development that follows further assumes that the leading-edge vortex is positioned above the wing surface all along the wing span. Thus, extreme camber cases where the leading-edge vortex can be shed below the wing surface at low angle of attack and may even roll around the leading edge to the upper surface at some spanwise location are not allowed.

The general equation for lift as resolved from the normal, $C_N$, and axial, $C_A$, forces is

$$C_L = C_N \cos \alpha - C_A \sin \alpha \quad (18)$$

Consistent with the current nomenclature, the total lift for the cambered planform (neglecting friction drag) then becomes

$$C_L = \left( C_{N_p} + \sum_{n=1}^{N} C_{T_n} \cos\phi_n / \cos \Lambda_n + C_Y - \sum_{n=1}^{N} C_{T_n} \tan \Lambda_n \right) \cos \alpha$$

$$+ \left( \sum_{n=1}^{N} C_{T_n} \sin\phi_n \right) \sin \alpha \qquad (19)$$

The angle $\phi$ is equal to the slope of the mean line perpendicular to the planform leading edge at the midpoint of the leading edge of each chordwise strip. Note that $C_T$ is defined as a positive force in the upstream direction.

Similarly, the total drag due to lift (neglecting friction drag) is given by

$$C_{D_L} = C_N \sin \alpha + (C_A)_{Suction} \cos \alpha \qquad (20)$$

or, for the cambered planform,

$$C_{D_L} = \left( C_{N_p} + \sum_{n=1}^{N} C_{T_n} \cos\phi_n / \cos \Lambda_n + C_Y - \sum_{n=1}^{N} C_{T_n} \tan \Lambda_n \right) \sin \alpha$$

$$- \left( \sum_{n=1}^{N} C_{T_n} \sin\phi_n \right) \cos \alpha \qquad (21)$$

The pitching moment is determined in much the same manner as that described previously for the uncambered planform. An additional term is required to account for the moment contribution of the suction-force component in the axial-force direction. The moment arm, $z_n$, for this force is the vertical distance from the

reference to the midpoint of each chordwise segment. The resulting equation is

$$C_m = C_{m_p} + \frac{1}{c}\left[\sum_{n=1}^{N}(C_{T_n}\cos\phi_n/\cos\Lambda_n)(x_n) + \sum_{m=1}^{M}\left(\sum_{1}^{N+1} C_{Y_2}\right)_m (x_m) + \sum_{n=1}^{N}(C_{T_n}\sin\phi_n)(z_n)\right] \tag{22}$$

where $C_{m_p}$ is the potential-flow moment resulting from the potential-flow normal forces only.

## EVALUATION AND RESULTS FOR THIN WINGS

Verification of the aerodynamic coefficient calculations for uncambered planforms has been accomplished through comparison with test data for delta, arrow, diamond, double-delta, rectangular, and ogee wings. Cambered wing calculations have been compared with data for a moderately cambered delta planform.

### Flat-Plate Wings

Data from reference 5 for delta and clipped delta planforms of taper ratio 0.0 and 0.4 are presented in figures 2 and 3. Results of the current method generally agree quite well with the data. However, the test data for the delta wing begin to depart significantly from the predictions when vortex breakdown reaches the wing trailing edge. Reference 6 reports that vortex breakdown occurs at 14 degrees angle of attack for the wing of figure 2. The delta wing (figure 2) exhibits little effect of vortex lift on the pitching moment. Apparently the leading-edge vortex lift is approximately equally distributed about the reference axis, which is at the quarter-chord of the mean aerodynamic chord. On the clipped delta wing of figure 3, the vortex-lift contribution to the moment becomes much more pronounced. The potential-flow results, considered alone, actually predict a moment in the wrong direction.

Comparisons between the theoretical results and data from reference 7 for an aspect-ratio-2.0 rectangular wing are presented in figure 4. Even though the predicted total lift agrees well with the data up to an angle of attack of 12 degrees, the data depart from the predicted moment at 8 degrees. This is attributed to the progression of the vortex across the planform as angle of attack is increased.

Comparisons with reference 6 data for an 80-/65-degree double-delta planform and an ogee planform are presented in figures 5 and 6. Excellent agreement with the lift and drag predictions is apparent to the angle of attack for vortex breakdown. Good agreement with the pitching moment is obtained at the lower angles of attack, but the data break away from theory before the angle of attack for vortex breakdown is reached. This could be caused by a complex flow interaction resulting from the formation of multiple leading-edge vortices on this type planform.

Figures 7 and 8 present test-to-theory comparisons for two planforms (reference 3) which help investigate the ability of the method to evaluate the effects of trailing-edge sweep. The lift of the clipped arrow wing of figure 7 is predicted very well, however the lift of the clipped diamond wing of figure 8 is under-predicted. This is attributed to the induced lift effect of the shed vo tex on the additional surface area aft of the trailing edge of the diamond wing tip.

Test data from a model which employs spanwise blowing on the wing upper surface (reference 8) is presented in figure 9 for a 30-degree delta wing. Comparison with predictions illustrates the potential of this method as a tool for estimating the benefits which can be realized from vortex augmentation of this type. The ability of the spanwise blowing to extend the leading-edge vortex lift to higher angles of attack is most pronounced. Agreement with the predicted lift-curve slope is apparent to angles of attack much above the no-blowing vortex breakdown region. There is a blowing-induced camber effect which is, of course, not predicted by the theory.

## Cambered Wings

The cambered-wing equations have been used to predict the characteristics of a moderately cambered ($C_{\ell_i} = 0.15$) delta wing for which reference 5 presents test data. The comparisons of

lift, drag, and moment shown in figure 10 indicate good agreement. The reference 5 data for the same wing with an uncambered section have been included in figure 10 to illustrate the method's ability to predict the incremental camber effect accurately. It is also noteworthy that the incremental vortex-lift contribution due to camber is very small. Thus, at least for small or moderate amounts of camber, the potential flow increment due to camber gives a good approximation for the incremental effects of camber.

## VORTEX-LATTICE ARRANGEMENT FOR THICK WINGS

Vortex-lattice methods are best suited for the analysis of thin wings with sharp leading edges which can be approximated by camber surfaces. The predicted results in general for this type of wing show good agreement with experimental data. However, when the vortex-lattice method is directly applied to thick wings (including multi-element wings) the calculated results do not agree with experimental data.

A typical conventional vortex-lattice layout for multi-element wings is shown in figure 11. Each wing element is represented by a network of horseshoe vortices lying on the camber surface and trailing behind the surface. As can be seen from this figure a bound vortex lies along the leading edge of each component of the multi-element system. This causes infinite velocities to be generated at the leading edge which produce very large negative pressure coefficients (unrealistic) at points in the immediate vicinity of the leading edge. This phenomenon is acceptable for thin sharp-leading-edge wings but fails to give acceptable predictions for thick wings. For example, the loads calculated for the F-111 wing in the high-lift configuration at angles of attack of 4 and 15 degrees are compared with experimental data (reference 9) in figures 12(a) and 12(b), respectively. Large discrepancies between experimental and theoretical loads are evident near the leading edge of the wing and flaps.

A technique for laying out the lattice has been developed at General Dynamics which greatly improves the pressure distributions predicted by the vortex-lattice method for thick multi-element wings. A typical example of this lattice is shown in figure 13. Each element of the multi-element wing is represented by a network of horseshoe vortices lying on and trailing behind a surface which is composed of the top surface and part of the

bottom surface, and wraps around the leading edge of the wing. The surface on the bottom is extended downstream of the anticipated stagnation point. If the surface is extended to the trailing edge the problem becomes singular and meaningless results are obtained. No large differences in predicted pressures have been noted for variations in the extent of the vortex sheet on the lower surface.

A large-aspect-ratio, unswept, untapered wing having the same section as the F-111 wing section at BL 289 was analyzed using this wrapped lattice arrangement. The pressure distributions calculated at the centerline of this wing are shown in figures 14(a) and 14(b) for angles of attack of 4 and 12 degrees, respectively. The chordwise distribution of the vortex lines is also shown in these figures. Since the pressures at the centerline of a large-aspect-ratio wing are compatible with two-dimensional flow results they are compared with two-dimensional experimental data (reference 10) and two-dimensional theoretical results (reference 11) in these figures. The predictions show good agreement with both the experimental and theoretical results. The two-dimensional theoretical pressure distributions shown were obtained with a much denser chordwise distribution of points. A better prediction should be obtained with the vortex-lattice method if a denser chordwise portioning of the lattice is employed.

## CONCLUDING REMARKS

A method has been formulated for determining the lift, zero-leading-edge-suction drag due to lift, and pitching moment of thin, sharp-edged, low-aspect-ratio wings with camber. This method utilizes a vortex-lattice procedure modified to include vortex-lift induced effects by including an extension of the Polhamus suction-analogy concept. Good agreement with experiment is obtained for simple highly swept planforms below the angle of attack at which vortex breakdown reaches the trailing edge of the wing and at somewhat lower angles of attack for wings with more complex flow patterns, such as double-delta and ogee planforms.

The method shows promise as a tool for evaluation of the potential of vortex augmentation systems.

To obtain more accurate predictions for the more complex planforms, it is necessary to include the effects of the

progression of the vortices away from the leading edge and tip of the planform and to include the vortex interactions on planforms which emanate multiple leading-edge vortices.

A method has also been developed for laying out the vortex lattice for thick multi-element wings which gives accurate pressure predictions on the top and part of the bottom surface of the wing. Comparison with experimental data and other theoretical methods substantiates the accuracy of the results.

## REFERENCES


1. Polhamus, E. C.: Predictions of Vortex-Lift Characteristics by a Leading-Edge Suction Analogy. Journal of Aircraft, volume 8, no. 4, April 1971, pp. 193-199.

2. Polhamus, E. C.: A Concept of the Vortex Lift of Sharp-Edge Delta Wings Based on a Leading-Edge Suction Analogy. NASA TN D-3767, December 1966.

3. Lamar, J. E.: Extension of Leading-Edge-Suction Analogy to Wings with Separated Flow Around the Side Edges at Subsonic Speeds. NASA TR R-428, October 1974.

4. Bradley, R. G.; Smith, C. W.; and Bhateley, I. C.: Vortex-Lift Prediction for Complex Wing Planforms. Journal of Aircraft, volume 10, no. 6, June 1973, pp. 379-381.

5. Emerson, H. F.: Wind-Tunnel Investigation of the Effect of Clipping the Tips of Triangular Wings of Different Thickness, Camber, and Aspect Ratio - Transonic Bump Method. NACA TN 3671, June 1956.

6. Wentz, W. H., Jr.; and Kohlman, D. L.: Wind Tunnel Investigations of Vortex Breakdown on Slender Sharp-Edged Wings. NASA CR-98737, November 1968.

7. Nelson, W. H.; and McDevitt, J. B.: The Transonic Characteristics of 22 Rectangular, Symmetrical Wing Models of Varying Aspect Ratio and Thickness. NACA TN 3501, June 1955.

8. Bradley, R. G.; Wray, W. O.; Smith, C. W.: An Experimental Investigation of Leading-Edge Vortex Augmentation by Blowing. NASA CR-132415, 1 April 1974.

9. Goss, W. J.: Report of Fourth Series Wind Tunnel Tests of the 1/6-Scale F-111 Semi-Span Model. Grumman Aircraft Report GW.TT 184 (310-4), October 1963.

10. Goodwin, L. C.: Wind Tunnel Tests on a 2-D Model of a NACA 64A210 (Modified) Section with Various Leading and Trailing Edge Devices, Using the Canadair 2-D Blowing Walls, in the NAE 6x9-Ft Low-Speed Wind Tunnel, NAE Test 6x9/0/40, DIR Project A11-Phase II, volumes 1, 2, and 3. Canadair Report ERR-CL-RAA-228-010, Sept. 1969.

11. Bhateley, I. C.: Investigation of Inviscid Incompressible Flow, Part IV: Potential Flow Analysis about Arbitrary Multiple Two-Dimensional Bodies by the Method of Distributed Singularities. General Dynamics Fort Worth Division Report ERR-FW-669, 31 March 1968.

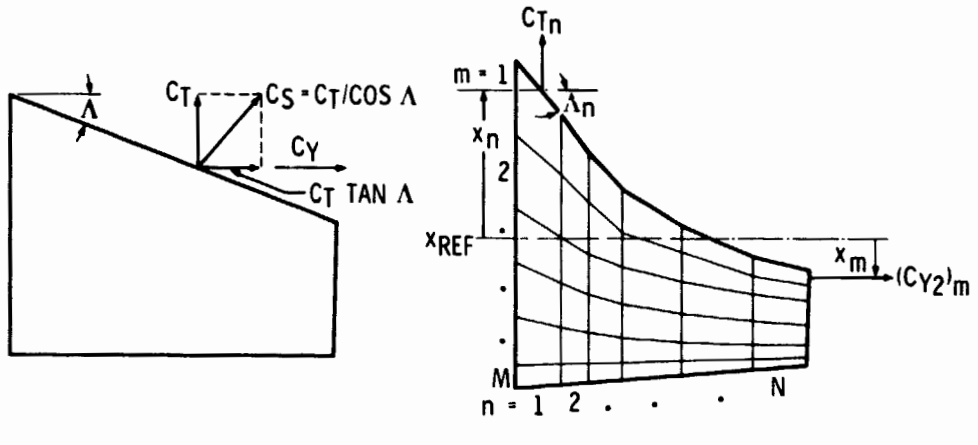


(a) Trapezoidal. (b) General.

Figure 1.- Potential-flow force coefficients from the vortex-lattice procedure.

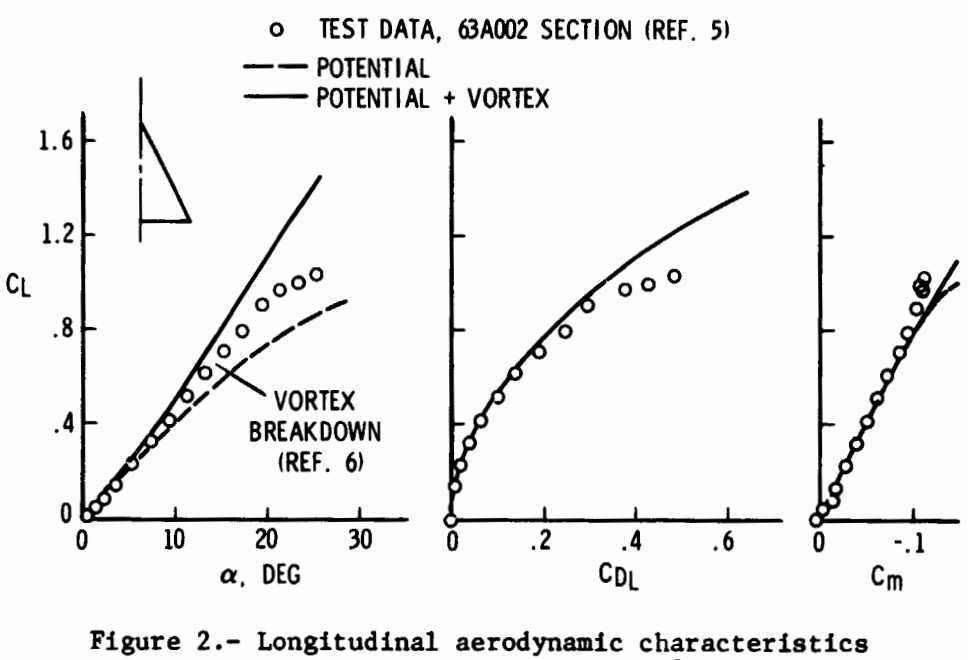


Figure 2.- Longitudinal aerodynamic characteristics of a delta wing with $\Lambda = 63^\circ$.

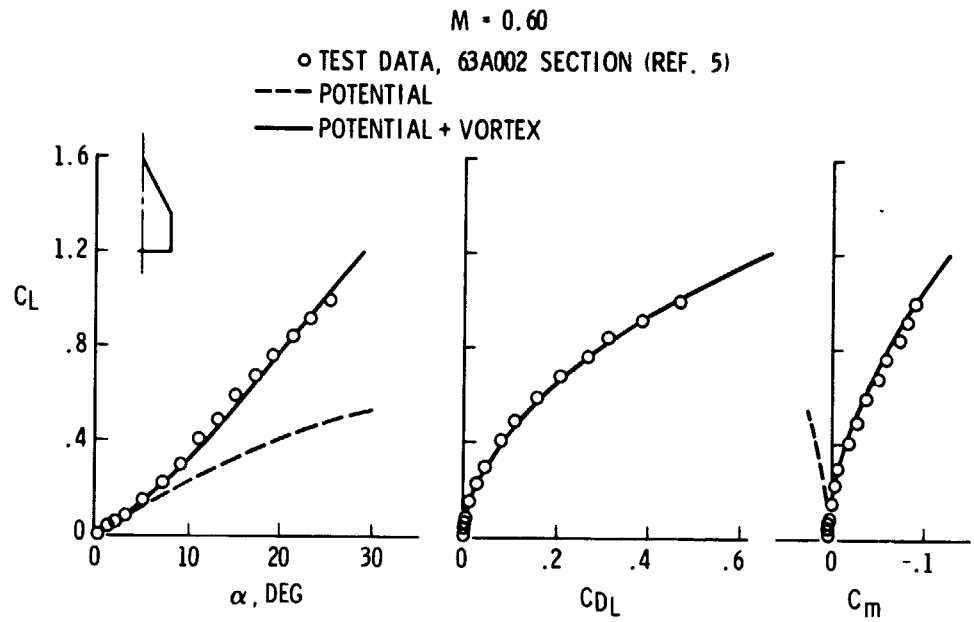


Figure 3.- Longitudinal aerodynamic characteristics of a clipped delta wing with $\Lambda = 63^{\circ}$ and $\lambda = 0.4$.

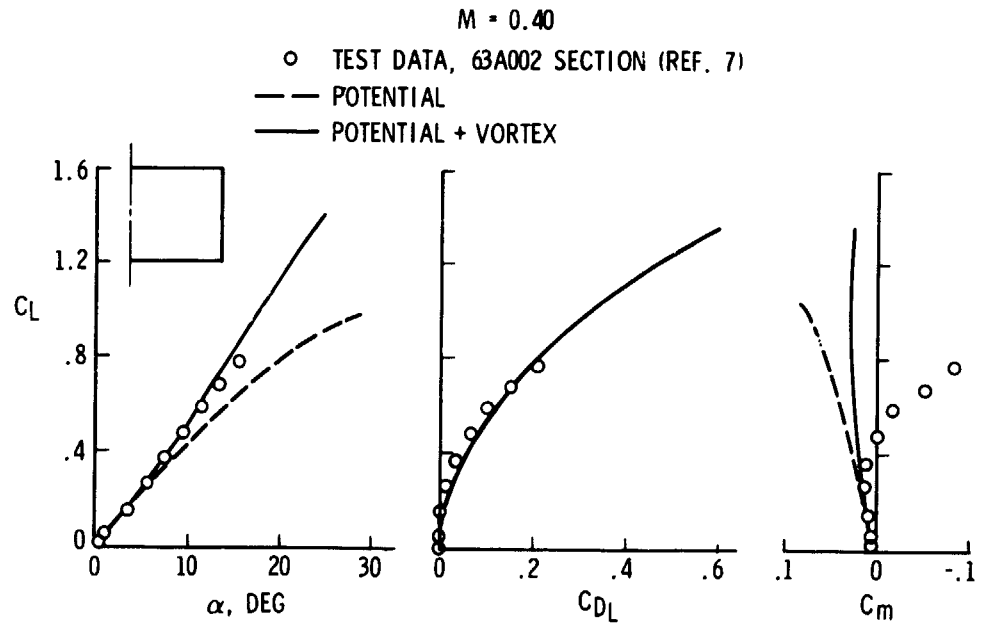


Figure 4.- Longitudinal aerodynamic characteristics of a rectangular wing with AR = 2.0.

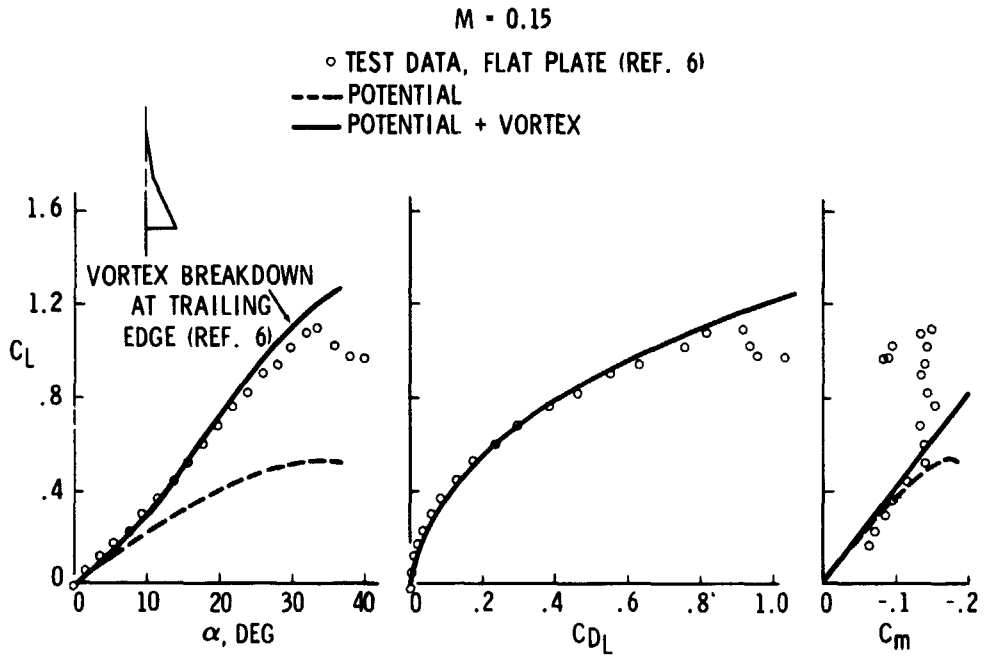


Figure 5.- Longitudinal aerodynamic characteristics of a double-delta wing with $\Lambda = 80^o/65^o$.

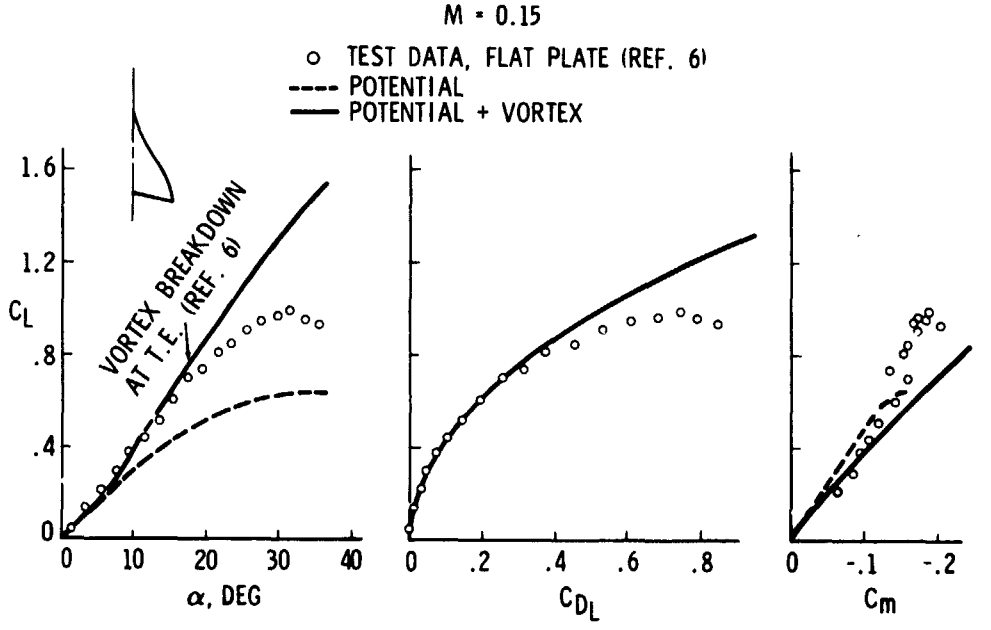


Figure 6.- Longitudinal aerodynamic characteristics of an ogee wing with AR = 1.7.

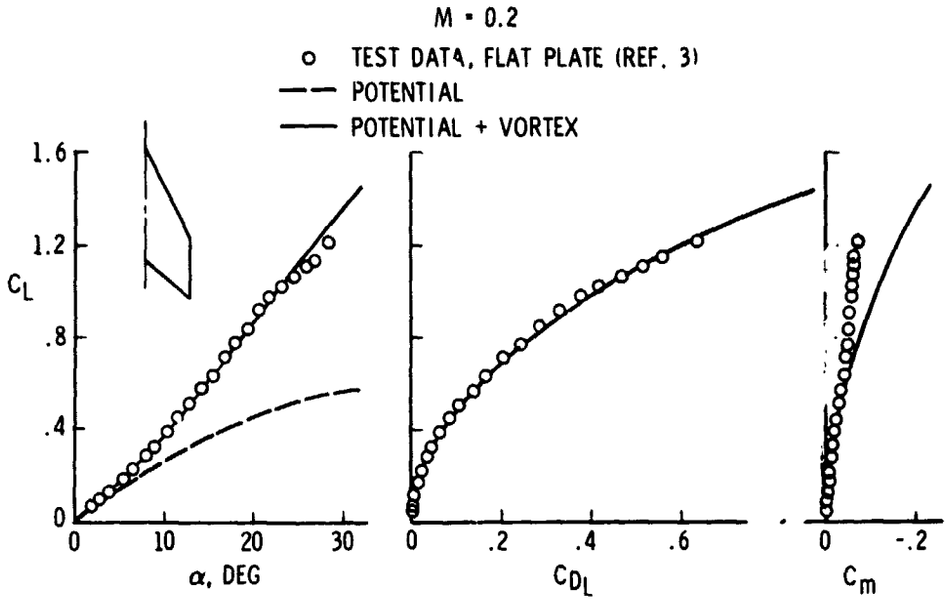


Figure 7.- Longitudinal aerodynamic characteris ics of a clipped arrow wing with $\Lambda = 63^{\circ}$.

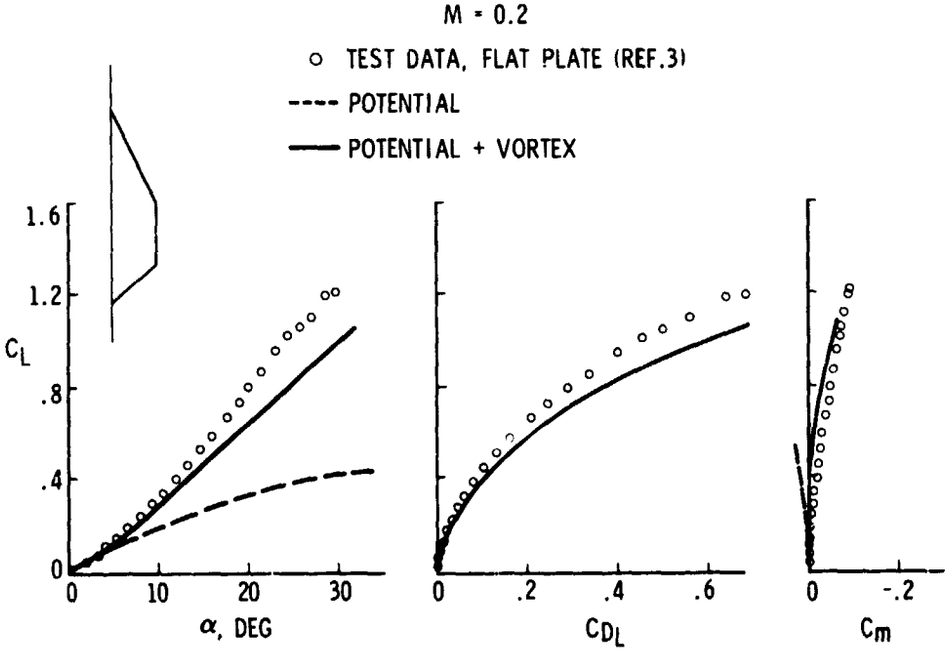


Figure 8.- Longitudinal aerodynamic characteristics of a clipped diamond wing with $\Lambda = 63^{\circ}$.

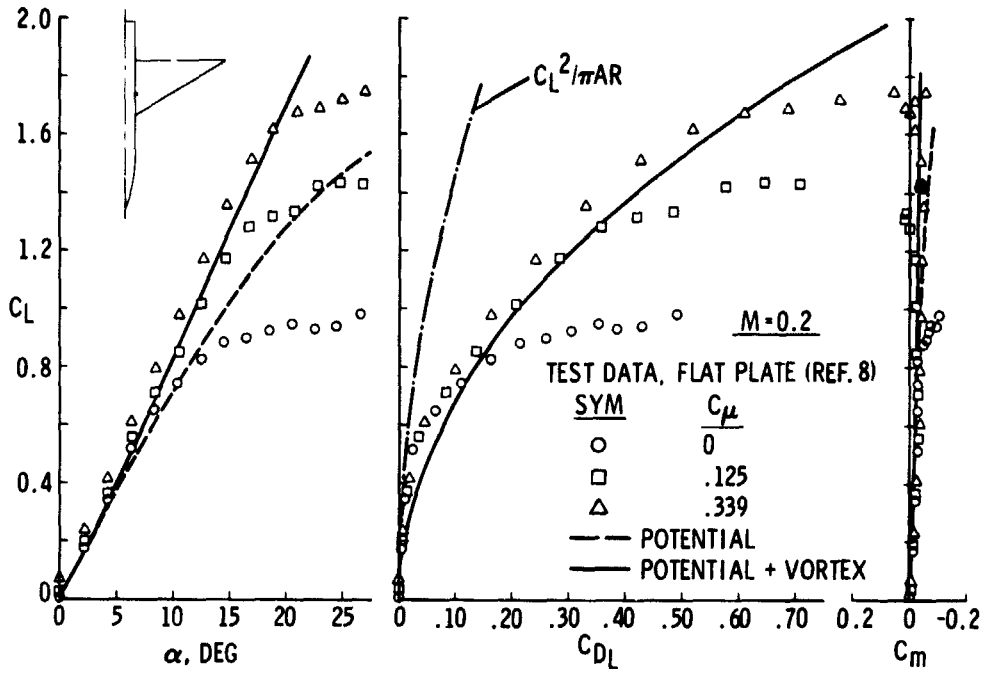


Figure 9.- Longitudinal aerodynamic characteristics of a delta wing with $\Lambda = 30^\circ$ and spanwise blowing.

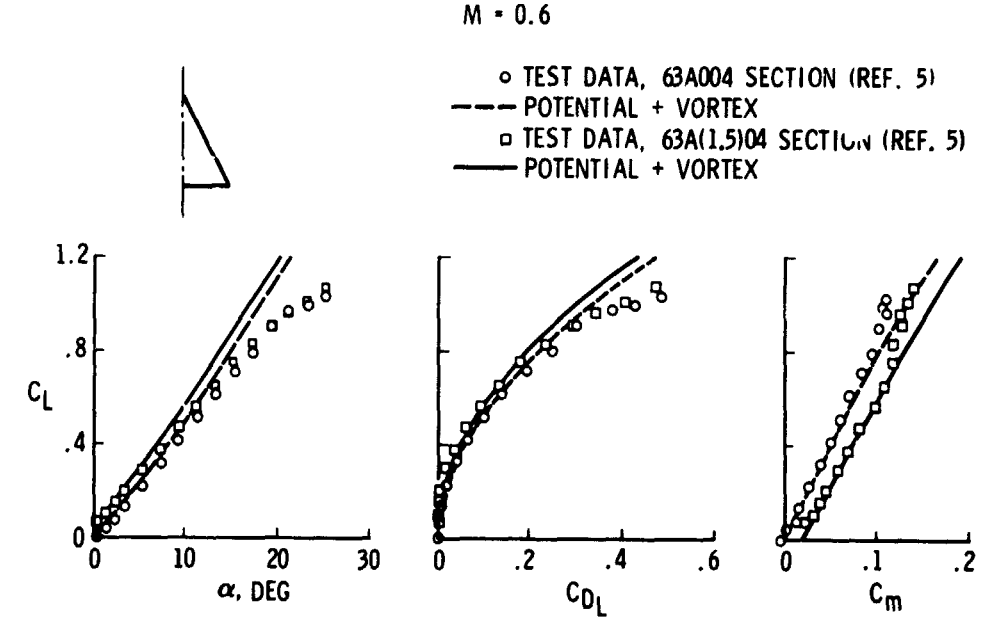


Figure 10.- Effect of camber on the longitudinal aerodynamic characteristics of a delta wing with $\Lambda = 63^\circ$.

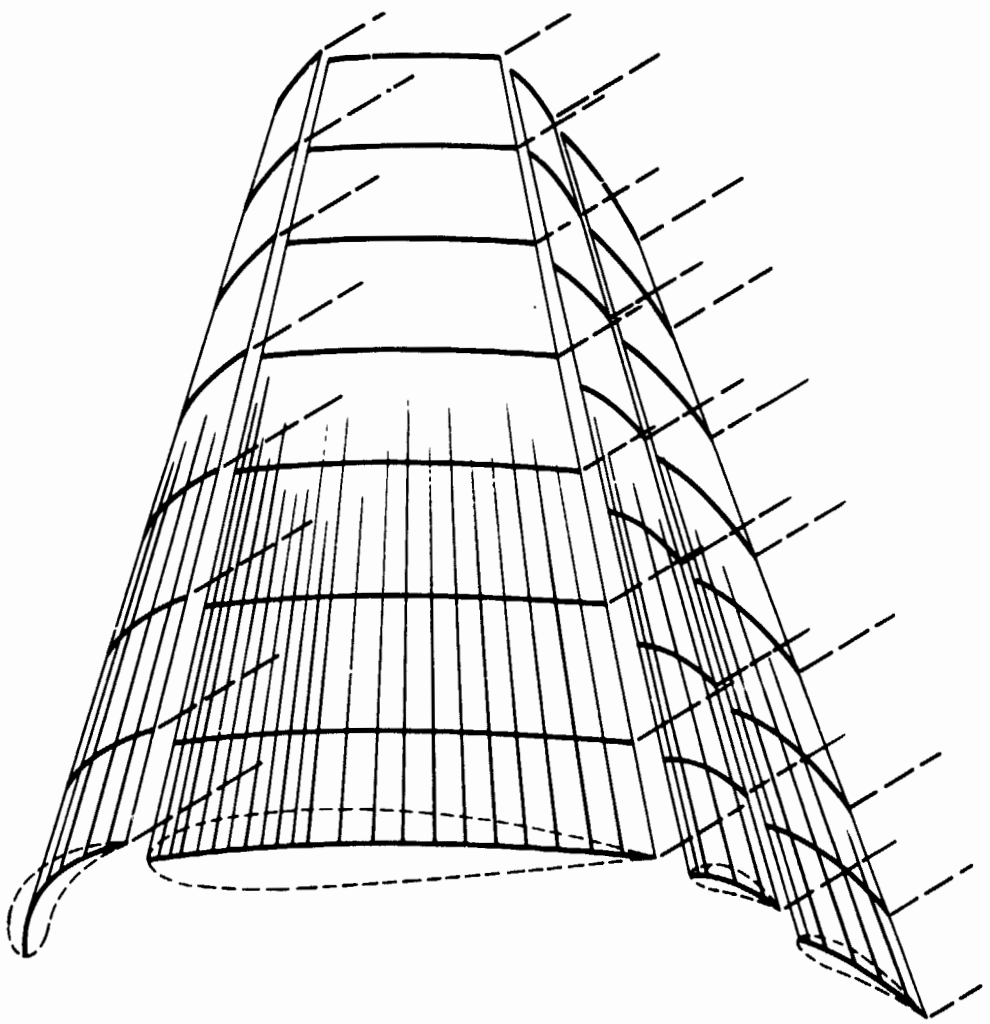

Figure 11.- Conventional vortex-lattice arrangement on a thick multi-element wing.

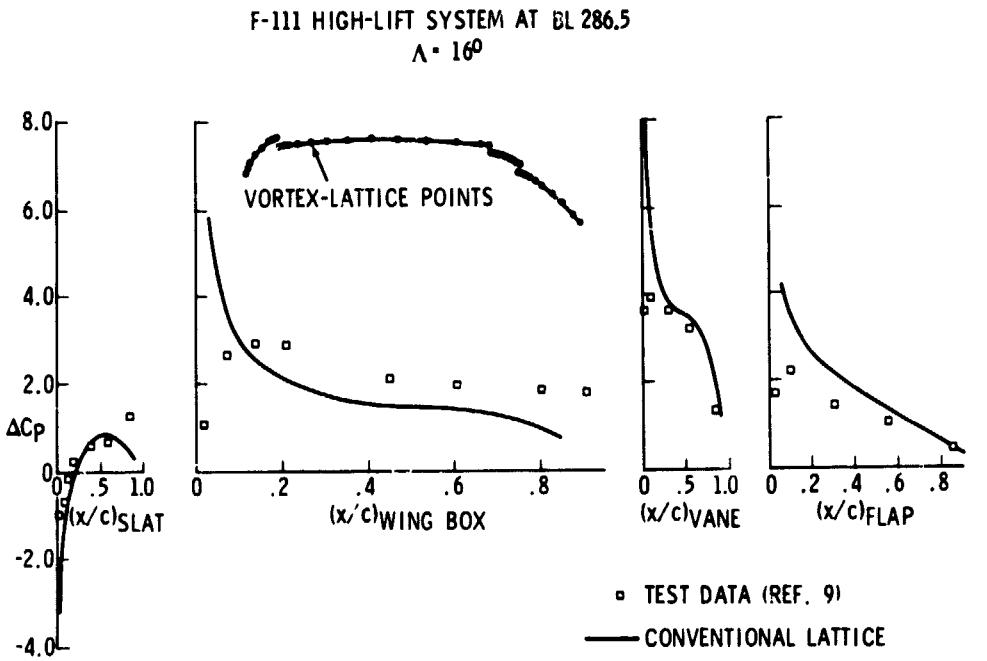


(a) $\alpha = 4^{\circ}$.

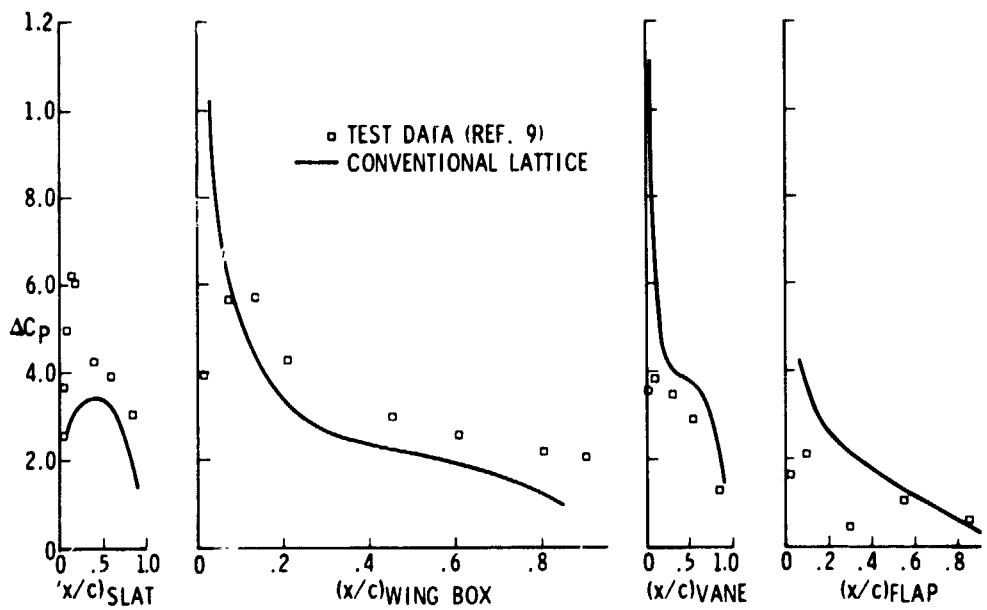


(b) $\alpha = 15^{\circ}$.

Figure 12.- Conventional vortex-lattice results compared with experimental pressure data on a thick multi-element wing.

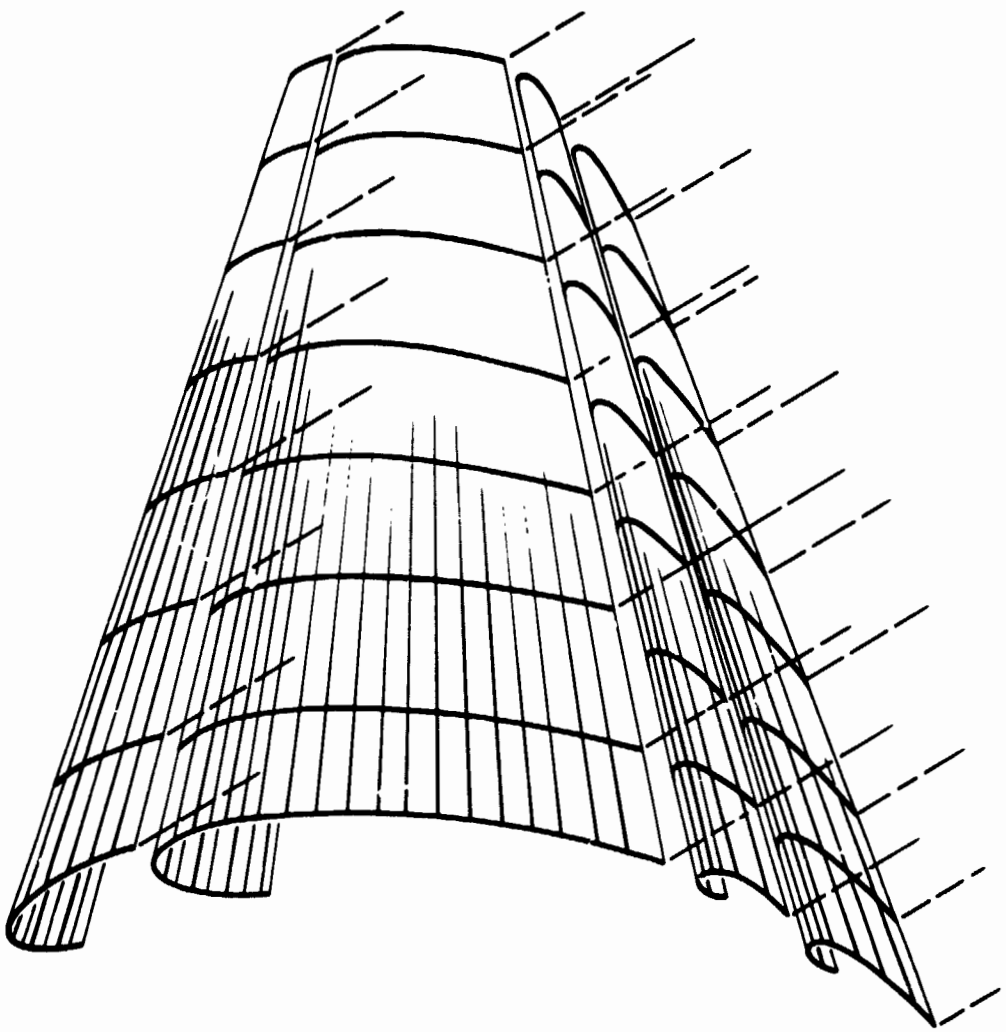

Figure 13.- Wrapped vortex-lattice arrangement on a thick multi-element wing.

F-111 HIGH-LIFT SYSTEM AT BL 289

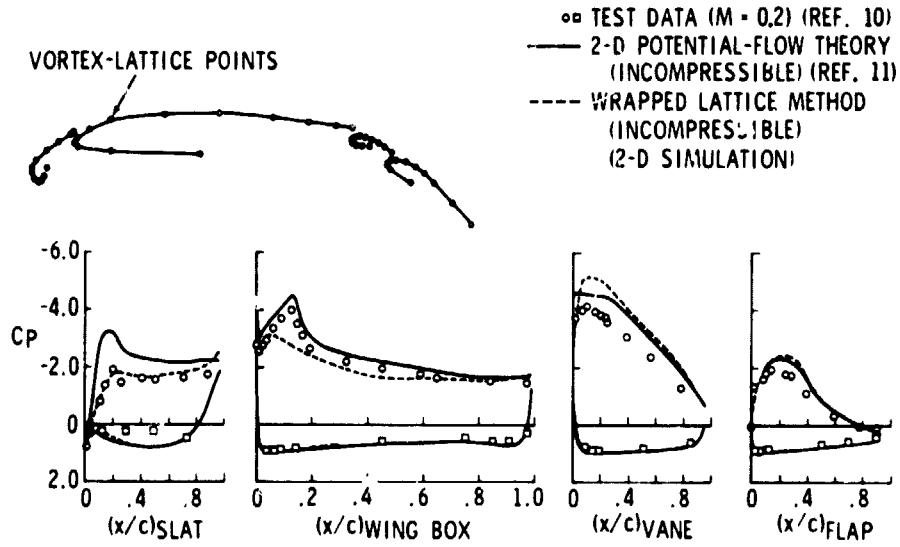


(a) $\alpha = 4^{\circ}$.

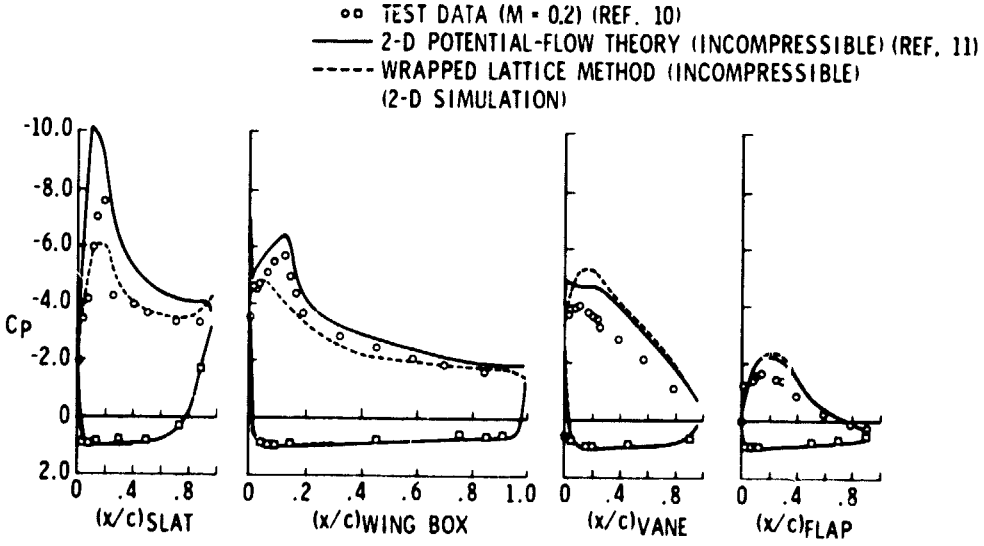


(b) $\alpha = 12^{\circ}$.

Figure 14.- Wrapped vortex-lattice results compared with experimental pressure data on a thick multi-element wing.